Facultad de Ciencias
Grado en Física

Trabajo Fin de Grado

Fluorescence Intensity Ratio and Whispering Gallery Mode techniques in optical temperature sensors. Comparative study.

Autora:
Franzette Paz Buclatin

Tutores:
Susana Ríos Rodríguez
Inocencio Rafael Martín Benenzuela

TABLE OF CONTENTS

ABSTRACT

Con el aumento del interés en los sensores ópticos de temperatura, muchos trabajos se han centrado en el estudio de distintos materiales ópticamente activos, como los vidrios dopados con tierras raras, para determinar el material más adecuado para ser desarrollado como sensor. En este trabajo, sin embargo, además del estudio de la capacidad de un vidrio de oxifluoruro dopado con Er^{3+} como sensor térmico, se ha realizado un estudio comparativo entre tres morfologías diferentes de un mismo material y el correspondiente método de detección empleado. En particular, se estudiaron un oxifluoruro dopado con Er^{3+} en forma de microesfera, fibra, y vidrio.

Las microesferas y las fibras presentan lo que se denomina Whispering Gallery Modes (WGM), que son resonancias producidas en el interior de una cavidad debido a múltiples reflexiones internas totales a lo largo de la superficie curva. Se han observado estas resonancias acopladas a la emisión típica de los iones de Er^{3+} cuando la muestra se excita con un láser. Además, se ha observado que estas resonancias se desplazan cuando las condiciones iniciales del entorno cambian. En particular, un cambio de temperatura provoca una dilatación térmica y una variación en el índice de refracción de la microesfera o de la fibra, que a su vez modifica las condiciones de resonancia de los WGM. Aprovechando este comportamiento de los picos de los WGM, se realizó una calibración de los desplazamientos con la potencia del láser y con la temperatura para la microesfera y la fibra.

Por otro lado, los iones de tierras raras presentan niveles de energía acoplados térmicamente en los que se produce una redistribución de población según la distribución de Boltzmann. La técnica denominada Fluorescence Intensity Ratio (FIR) utiliza la dependencia térmica de la relación de intensidades de estos niveles para calibrar la temperatura de la muestra. Para el caso de los iones de Er^{3+}, los niveles acoplados térmicamente son $^2H_{11/2}$ y $^4S_{3/2}$. Se realizó una calibración de temperatura utilizando esta técnica para el vidrio de la misma composición.

Para comparar las tres morfologías se utilizaron dos parámetros: la sensibilidad relativa y la incertidumbre en la temperatura. A través del análisis de los desplazamientos de los WGM se obtuvo una sensibilidad relativa de 9.9×10^{-5} K^{-1} para la microesfera y también para la fibra. Por otro lado, a través de la técnica FIR, el vidrio registró una sensibilidad relativa de 1.0×10^{-2} K^{-1}, dos órdenes de magnitud superior a la de los microresonadores. Por otro lado, se obtuvo una incertidumbre en la temperatura un orden de magnitud menor para la microesfera (0.11 K) y la fibra (0.37 K) para la banda de 670 nm, con respecto al vidrio (1.8 K).

Los resultados de este estudio facilitan la selección de la morfología de un material ópticamente activo y el método de detección correspondiente a la hora de desarrollar un sensor óptico de temperatura.

With the growing interest in optical temperature sensors, many works have been focused in studying various optically active materials, such as trivalent rare earth doped glasses, in order to determine the most suitable material to be developed as a sensor. In this work, however, aside from the characterization of the thermal sensing capabilities of an Er^{3+} doped oxyfluoride glass, a comparative study between three different morphologies of the sample and the corresponding sensing method used has been performed. In particular, an Er^{3+} doped oxyfluoride microsphere, fiber, and bulk glass were studied.

Microsphere and fibers are known to support what is called whispering gallery modes (WGM), which are resonances produced in the interior of a resonator due to successive total internal reflections along its curved surface. Experimentally, these resonances were observed coupled to the typical emission of Er^{3+} ion when the sample was excited with laser. Moreover, it has been observed that these resonances experience a shift when the initial conditions of the surrounding medium change. In particular, a change in temperature produces a thermal dilation and a change in the refraction index of the microsphere or fiber, which in turn changes the resonance condition of the WGM. Based on this behavior, the WGM shifts of a microsphere and fiber were calibrated as a function of pump power and temperature.

On the other hand, trivalent rare earth ions are known to have thermally coupled energy levels in which a thermal redistribution of population occurs following that of Boltzmann's distribution. The Fluorescence Intensity Ratio (FIR) technique utilizes the thermal dependence of the intensity ratio of these thermalizing levels in order to calibrate the temperature of the sample. For the case of Er^{3+} ion, the thermally coupled levels refer to $^2H_{11/2}$ and $^4S_{3/2}$. A temperature calibration using this technique was done for the bulk glass of the same composition.

In order to compare the performance of each sample, the relative sensitivity and temperature uncertainty were determined. Through the WGM displacement analysis, a relative sensitivity of 9.9×10^{-5} K^{-1} was obtained for the microsphere, a value theoretically valid also for the fiber. On the other hand, through the FIR technique, the bulk glass recorded a relative sensitivity of 1.0×10^{-2} K^{-1}, two orders of magnitude greater than that of the microresonators. On the other hand, the microsphere and fiber presented temperature uncertainties for the 670 nm band an order of magnitude lower than that of the bulk glass: 0.11 K, 0.37 K, and 1.8 K respectively.

The results of this study facilitate the selection of the morphology of an optically active material and the corresponding sensing method to be employed in the development of an optical temperature sensor.

1. INTRODUCTION

En este capítulo se presentarán las motivaciones de este trabajo, y se comentarán algunos de los avances realizados en la disciplina en la que se enmarca este trabajo. El objetivo principal es el estudio de la capacidad de diferentes formas de vidrio de oxifluoruro dopado con iones de Er^{3+} como sensor de temperatura mediante el análisis de los desplazamientos de los WGM y la técnica FIR. El trabajo está motivado por el gran interés en el desarrollo de los sensores ópticos hoy en día debido a sus ventajas frente a los sensores eléctricos convencionales. Además, los iones de tierras raras en su forma trivalente, como el ion Er^{3+}, son comúnmente empleados en estos estudios ya que presentan líneas de transición prominentes en la región visible e infrarroja cercana y también son compatibles para los estudios con FIR. En cuanto al material huésped, se eligió el vidrio de oxifluoruro debido a sus buenas propiedades ópticas, característica de los vidrios de fluoruro, así como por su estabilidad química y mecánica, característica de los vidrios de óxido. El método de detección asociado a cada sensor óptico de temperatura varía de uno a otro, dependiendo de la muestra estudiada. Por lo tanto, también sería importante evaluar la eficiencia de cada método, en este caso, uno basado en los desplazamientos de los WGM y el otro basado en la técnica FIR, con el objetivo de determinar qué morfología del material y método son los más adecuados para el desarrollo de un sensor óptico de temperatura.

In this chapter, the motivations behind this work as well as an account of related works in the same field will be presented. This work aims to study the potential of different forms of Er^{3+} doped oxyfluoride glass as temperature sensors through the analysis of WGM displacements and the FIR technique. This stems from the amount of attention on the development of optical sensors nowadays due to their advantages over conventional electrical-based sensors. Furthermore, rare-earth ions in their trivalent form, such as Er^{3+}, are typically the subject of such works since they present prominent transition lines in the visible and near infrared region and they are also compatible for FIR studies. As for the host material, oxyfluoride glass was chosen due to its good optical properties, characteristic of fluoride glasses, as well as for its stable chemical and mechanical properties, characteristic of oxide glasses. The sensing method behind the numerous works on optical temperature sensors varies from one work to another, depending on the sample studied. Therefore, another matter of interest would be to evaluate the efficiency of each method, in this case, one based on the WGM displacements and the other based on the FIR technique, to determine which morphology of the material and method is best suitable for the development of an optical temperature sensor.

Optical sensors operate by detecting changes in the intensity, phase, polarization, wavelength or spectral distribution of the light beams as they interact with the surrounding medium. This type of sensor provides more efficiency due to their exclusive

features accounting from their light-based detection mechanism [1]. Unlike conventional sensors, optical sensors offer electrical passiveness, greater sensitivity, immunity from electromagnetic interference, large bandwidth, both point and distributed configurations and multiplexing capabilities [2]. Moreover, optical sensors in the form of nanoparticles and microspheres permit non-invasive measurements through remote sensing mechanisms. In this way, the sensor is deposited into the sample, an external perturbation is made, and the sensor response is detected externally [3].

Rare earth ions are usually employed in the development of optical sensors due to their interesting optical properties. In particular, the trivalent form of the lanthanide series has been used in numerous research works and so their optical properties are relatively well-known [4]. They are easily obtainable and present absorption bands within the emission spectrum of readily available pump sources. Additionally, they present prominent transition lines in the visible and near infrared region and due to the screening of outer electrons, their energy level structure only varies slightly between different host materials [5]. They also have thermally coupled levels which are of interest for the Fluorescence Intensity Ratio (FIR) technique to be discussed later. Particularly, the Er^{3+} ion has the thermally coupled $^2H_{11/2}$ and $^4S_{3/2}$ levels. It is one of the most used rare earth ions due to its applications as a fiber amplifier for the 1.5 μm telecommunication range [6] and for the upconversion lasers of visible green emission [7]. Moreover, it presents emission lines in the near infrared region where the biological tissue is transparent, thus, it can also be used in biomedicine.

In the design of optical devices, the host material is also an important factor to consider since their vibrational properties can influence the optical behavior of the dopant ion. Many of the transition lines of practical importance of rare earth ions originate from excited levels with small energy gap. Therefore, in order for the radiative transitions of the active ions to dominate the non-radiative loss, materials with lower phonon energy are recommended as hosts. With this in mind, fluoride glasses are good candidates due to their low phonon energy (300 – 400 cm^{-1}). However, because of their low chemical and mechanical stabilities, fluoride glasses are difficult to fabricate. On the other hand, oxide glasses generally have better chemical and mechanical stabilities but higher phonon energy (1100 cm^{-1}). Thus, oxyfluoride glasses are expected to have excellent optical properties and good mechanical and chemical stability resulting from the compromise between pure fluoride and oxide glasses [8,9].

Temperature is a parameter of great importance in the industry and many scientific processes. In particular, on the cellular level, temperature strongly influences the form and function of macromolecules and cells. Thus, manipulation of these microsystems can be made possible through a precise and accurate control of temperature [10].

With this in mind, the main objective of this work is to study the potential of an Er^{3+} doped oxyfluoride glass as an optical temperature sensor. Two techniques are usually employed, the study of Whispering Gallery Modes (WGM) displacements [11–15] when

using a microresonator and the FIR technique when using lanthanide-doped materials [16–19]. In this work, a comparative study of the efficiency of each technique for the same Er^{3+} doped precursor glass will be performed.

The FIR technique consists on the study of the ratio between the fluorescence intensity of two thermally-coupled levels as a function of temperature. Thermally-coupled levels refers to two closely separated energy levels wherein the higher level is populated as the temperature increases. The population of the thermally-coupled levels follows the Boltzmann distribution [19]. The first reported work of Er^{3+} doped FIR calibration using the thermally coupled levels $^2H_{11/2}$ and $^4S_{3/2}$ was done by Berthou and Jörgensen in 1990 [20]. In this work, Er^{3+} doped fluoride glass accounted for an accuracy of 2 K when used as a temperature sensor in the temperature range of 20 to 200 ºC. The main drawback of this sensor lies in the maximum operating temperature of approximately 250 ºC due to the use of fluoride glass as the host material.

On the other hand, microresonators have also attracted interest due to their high-accuracy measurements, originating from the confinement of light beams, and their small dimensions suggesting biotechnological applications. In particular, dielectric structures with circular symmetry, such as microspheres or optical fibers, constitute an emerging class of resonators because they support the so-called Whispering Gallery Modes. WGM refers to the confinement of a wave field inside the resonator, particularly along its inner surface, due to successive internal reflections. When the wave field returns in-phase to its starting point, WGM resonances are produced. Since this phenomenon is highly dependent on the morphological structure (i.e. size and geometry) and dielectric properties (i.e. refractive index), changes in the position of the WGM resonances are associated to changes in these magnitudes produced by a change in the original conditions of the surrounding medium. This principle is the foundation of WGM-based optical sensors. Various works have been published using WGM as an optical sensor to measure pressure [21], humidity [22], and temperature [11–15] among others.

2. AIM OF THIS WORK

El objetivo de este trabajo es estudiar el desplazamiento con la temperatura de las resonancias WGM de la microesfera y de la fibra, y estudiar el efecto de termalización en el vidrio, todo hecho de la misma matriz de oxifluoruro dopado con iones de Er^{3+}. Este estudio permitirá determinar cuál de las morfologías consideradas es más apropiada para ser utilizada como sensor de temperatura.

This work aims to study the displacement with the temperature of the WGM resonances of the microsphere and fiber and to study the thermalization effect on the bulk glass from the same precursor Er^{3+} doped oxyfluoride glass. The results obtained in this study will allow the selection of the morphology with a better performance to be used as a temperature sensor. To accomplish that, the following steps will be carried out:

- Observe the emission bands of Er^{3+} with the excitation of a 532 nm laser.
- Detect the WGM resonances in a microsphere and optical fiber made of Er^{3+} doped glass.
- Characterize the pump power dependence of WGM resonance shifts.
- Calibrate the temperature dependence of WGM resonance shifts
- Characterize the wavelength dependence of WGM resonance shifts.
- Study the thermalization effect on the of Er^{3+} doped bulk glass emission using the FIR technique.
- Compare the performance of WGM shifts of the microsphere and optical fiber, and the thermalization effect in the bulk glass to determine the most efficient method and morphological structure for the development of an Er^{3+} doped oxyfluoride glass temperature sensor.

3. THEORETICAL BACKGROUND

Para poder comprender e interpretar los resultados obtenidos en el procedimiento experimental, es necesario explicar primero los conceptos científicos utilizados a lo largo de este trabajo. Este capítulo comenzará con la introducción de las propiedades ópticas de los iones de tierras raras, así como algunas propiedades interesantes del erbio. A continuación, se discutirá el fundamento teórico detrás de los WGMs y del método FIR, así como su aplicación para la medida de temperatura. Por último, se presentarán los parámetros utilizados comúnmente para caracterizar los sensores térmicos.

To be able to understand and interpret the results obtained from the experimental procedure, it is necessary to first explain the scientific concepts applied throughout this work. This chapter will start with the introduction of general optical properties of rare-earth ions, as well as some interesting properties of erbium. Next, the physics behind the WGMs and the FIR method as well as how they are used for temperature sensing will be discussed. Lastly, the parameters used to characterize thermal sensors will be presented.

3.1 Rare-Earth Ions: Erbium

Rare-earth ions are often used in the development of active optical materials due to their sharp fluorescent transition lines in the visible and near infrared region. The ground state electronic configuration of rare-earth ions is similar to that of Xenon but with electrons in its inner *4f* subshell. In particular, the electronic configuration for Erbium is as follows:

$$\text{Er:} \qquad \dots 4f^{12}5s^{2}5p^{6}6s^{2}$$

with the first nine subshells up to $4d^{10}$ completely filled.

Rare-earth ions in crystals are usually in trivalent form, wherein it loses its two outermost electrons in *6s*, one of its *5d* electron if there is one, otherwise, one of the electrons in *4f*. The trivalent electronic configuration of erbium is given by:

$$\text{Er}^{3+}\text{:} \qquad \dots 4f^{11}5s^{2}5p^{6}$$

The fluorescent lines are produced by the transitions between the partially filled *4f* levels. Moreover, since the *4f* subshell is shielded by the *5s* and *5p*, the emission lines are relatively narrow and the energy level structure is weakly dependent on the host material. [5]

Erbium is of particular interest in the optical field due to its emissions in the near infrared region. Here lies what are called biological windows in which the biological tissue has the lowest absorption, thus, suggesting possible medical applications for erbium-doped materials.

3.2 Whispering Gallery Modes

Whispering Gallery Modes is the term given to the resonances of a wave field inside a cavity due to the successive total internal reflections on its curved surfaces. In this work, electromagnetic WGM in dielectric resonators such as optical fibers and microspheres will be studied.

For total internal reflections to occur, the refractive index of the resonator (n) should be greater than that of the surrounding medium (n') and this condition will be complied if:

$$\theta_i > \theta_c = \sin^{-1}\left(\frac{n'}{n}\right) \quad (1)$$

where θ_i is the incident angle of the ray of light and θ_c is the critical angle. Due to the cylindrical symmetry and spherical symmetry of the fiber and microsphere respectively, all subsequent incident angles are the same and the light is trapped inside the cavity. For this reason, these resonators have high Q-factors (i.e. low losses). If $\theta_i \approx \frac{\pi}{2}$, then the light will travel close to the surface. When the light returns to the starting point in phase (2π), a constructive interference occurs giving rise to WGM resonances. The resonance condition for a resonator of radius $R \gg \lambda$ is given by [23]:

$$2\pi Rn = l\lambda \quad (2)$$

where l is the number of wavelengths that fits in the circumference and can be identified as the polar mode number.

Apart from the geometric properties of the resonator such as the shape and size, the WGM also greatly depend on its composition, particularly on its refractive index. Larger refractive index change between the resonator and the medium contributes to a higher Q-factor, while lower refractive index change increases the sensitivity of the sensor to its surrounding medium [24].

3.3 Temperature sensors

The operation of optical temperature sensors relies on the variation of its optical properties due to a change in its surrounding environment due to temperature. It is a topic of interest nowadays since the temperature can be remotely measured, they can be

employed for very small-scale temperature sensing, and the detected signal is not perturbed by the electromagnetic interferences unlike typical thermometers. In order to develop such sensors, WGM displacement technique and Fluorescence Intensity Ratio (FIR) technique are often employed.

3.3.1 WGM displacement technique

This technique is only applicable for microresonators that geometrically support WGM, such as microspheres or optical fibers. The size and refractive index of the resonator can vary depending on the thermodynamic conditions of its surrounding medium, such as temperature, pressure, or humidity. These changes will be reflected on the resonant wavelength, reason why they are often used as thermal [11–15], pressure [21], or humidity sensors [22] among others. In particular, from Equation (2) the following expression showing the dependence of the resonant wavelength with the temperature is obtained:

$$\frac{d\lambda}{dT} = \left(\frac{1}{R}\frac{\partial R}{\partial T} + \frac{1}{n}\frac{\partial n}{\partial T}\right)\lambda \tag{3}$$

Identifying $\alpha = \frac{1}{R}\frac{\partial R}{\partial T}$ as the thermal expansion coefficient and $\beta = \frac{1}{n}\frac{\partial n}{\partial T}$ as the thermo-optic coefficient of the material, a more explicit expression describing the WGM displacements can be derived from Equation (3) as follows:

$$\Delta\lambda = (\alpha + \beta)\lambda\,\Delta T \tag{4}$$

wherein $\Delta\lambda$ represents the WGM displacement and ΔT the temperature change. Since both coefficients are generally positive for glasses [25,26] a redshift of the resonant peaks as the temperature increases is expected as can be seen in Figure 1. This technique relies on this peak shift in order to determine the temperature of the surrounding medium.

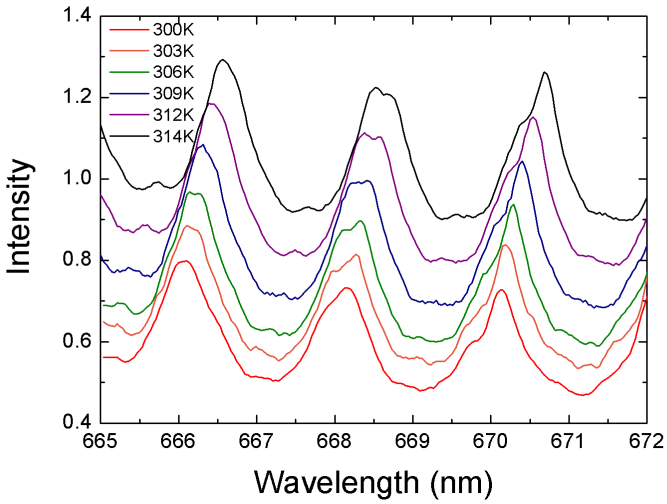

Figure 1. Shift of WGM peaks with an increase of temperature

3.3.2 Fluorescence Intensity Ratio

The FIR technique consists of analyzing the fluorescence intensity of thermally coupled energy levels to determine the temperature of the material. Thermally coupled energy levels refers to two closely separated levels in thermal equilibrium. Due to the small energy gap between the two levels, the atoms in the lower level can be promoted to the upper level with the increase of temperature through non-radiative mechanisms. This thermal redistribution of population follows the Boltzmann distribution given by the following equation [4,27]:

$$R = \frac{N_2}{N_1} = \frac{I_{20}}{I_{10}} = \frac{g_2 A_{20} h\nu_2}{g_1 A_{10} h\nu_1} \exp\left(-\frac{\Delta E}{kT}\right) = B \exp\left(-\frac{\Delta E}{kT}\right) \quad (5)$$

$$B = \frac{g_2 A_{20} h\nu_2}{g_1 A_{10} h\nu_1}$$

where N_i, I_{i0}, g_i, A_{i0},ν_i are the population, the fluorescence intensity, the degeneracy, the spontaneous emission rate and angular frequency of the transition from the lower (i = 1) and upper (i = 2) thermally coupled levels to the terminal level 0; ΔE is the energy gap, h is the Planck's constant, k is the Boltzmann constant, and T is the absolute temperature of the material.

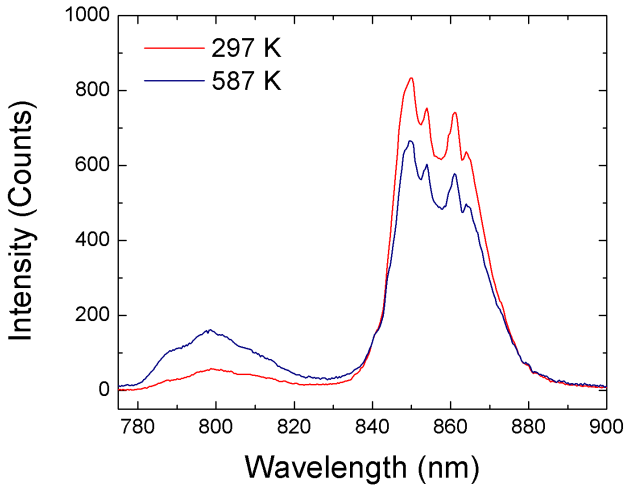

Figure 2. Change in relative spectrum intensities for the 800 nm and 850 nm emission bands of Er^{3+} ions for different temperatures

The use of thermally coupled levels for FIR is advantageous since their individual population is directly proportional to the total population, thus, the ratio obtained will be independent of the excitation power. It is also important to consider the energy gap of these levels in developing a temperature sensor. This gap is highly dependent of the host material. In particular, for a silica-based glass host, the energy gap should be from 200 cm^{-1} to 2000 cm^{-1}. Lower energy gaps will result in overlapping emission bands and higher energy gaps will make it harder to populate the higher energy level, thus reducing

the efficiency of this technique. In addition, the thermally coupled levels should be 3000 cm^{-1} above the next lower level for the radiative transitions to dominate over the non-radiative ones [28].

3.3.3 Sensor performance

Sensor performance is usually described through the relative sensitivity and temperature uncertainty. In general, the relative sensitivity is defined as the rate at which the measured parameter (MP) changes due to a variation in temperature and is defined as [14]:

$$S_{rel} = \frac{1}{MP}\frac{d\,MP}{dT} \tag{6}$$

Since this parameter does not depend on the nature of the sensor, it has been used as the figure of merit to compare different temperature sensors.

For a thermal sensor based on the WGM displacements, MP corresponds to the resonant wavelength and for one based on FIR, it corresponds to the intensity ratio. Using Equations (3) and (5), a more straightforward expressions for the sensitivities are obtained.

$$S_{WGM} = \frac{1}{\lambda}\frac{d\lambda}{dT} = \alpha + \beta \tag{7}$$

$$S_{FIR} = \frac{1}{R}\frac{dR}{dT} = \frac{\Delta E}{kT^2} \tag{8}$$

On the other hand, the temperature uncertainty refers to the minimum temperature change that can be detected in a given measurement. Assuming that this change originated only from the changes in the measured parameter, δT is given by the following expression:

$$\delta T = \frac{1}{S_{rel}}\frac{\delta MP}{MP} \tag{9}$$

where δMP refers to the uncertainty of the measured parameter. This shows that δT is a function of the physical phenomena behind the sensor operation, quantified by S_{rel}, and of the experimental setup.

Temperature uncertainties can be experimentally estimated by measuring MP several times under the same conditions, obtaining δMP as the standard deviation of the distribution, and substituting its value in Equation (9). It can also be obtained by calculating the temperature associated to each value of MP measured and studying their statistical distribution [29].

4. METHODOLOGY

En este capítulo se describen los procedimientos experimentales utilizados para el desarrollo y caracterización de diferentes formas (microesfera, fibra y vidirio) de oxifluoruro dopado con iones de Er^{3+}como sensores ópticos de temperatura. Como se discutió en el capítulo anterior, se utilizó la técnica de desplazamiento de los WGM para la calibración de la microesfera y de la fibra óptica, mientras que el FIR se utilizó para la calibración de temperatura del vidrio. El estudio del desplazamiento de los WGM se realizó de dos maneras: en función de la potencia de excitación del láser y en función de la temperatura. En primer lugar, se detallará la producción del vidrio, fibra y microesfera de oxifluoruro dopado con Er^{3+} y, a continuación, se describirá el montaje experimental de cada técnica.

In this chapter, the experimental procedures followed in order to develop and characterize different morphologies (microsphere, fiber, and bulk glass) of Er^{3+} doped optical temperature sensor will be described. As discussed in the previous chapter, WGM displacement technique was used for the calibration of microsphere and optical fiber while FIR was used for the temperature calibration of the bulk sample. The study of the WGM displacement was done in two ways: as a function of the laser pump power and as a function of temperature. First, the production of the Er^{3+} doped oxyfluoride glass, fiber and microsphere will be detailed and afterward, the experimental setup for each technique will be described.

4.1 Production of Er^{3+} doped samples

All the samples studied in this work were obtained from the same matrix of Er^{3+} doped oxyfluoride glass. From here, microspheres and optical fibers were fabricated.

4.1.1 Er^{3+} doped oxyfluoride glass

The bulk sample of the Er^{3+} doped oxyfluoride glass used in this work was produced in the laboratory of 'Espectroscopía Láser y Altas Presiones' of the University of La Laguna [30]. It was prepared with a molar composition in mol%: 30 SiO_2, 15 Al_2O_3, 29 CdF_2, 22 PbF_2, 1.5 YF_3, and 2.5 ErF_3. The glass was produced melting the precursor component at 1050ºC for two hours and then the molten glass was poured onto a stainless-steel plate at room temperature to solidify.

4.1.2 Optical fiber

The optical fiber was produced by continuously depositing the same molten glass matrix described previously in a rotating mechanism. In this way the melt is stretched, and the cylindrical form of the fiber is obtained.

4.1.3 Microsphere

Microspheres can be easily produced through various methods such as polishing, chemical etching, rapid quenching of liquid droplets [31], or melting the tip of an optical fiber [32]. The microspheres studied in this experiment were obtained by rapid quenching of liquid droplets. First, the bulk glass was crushed and dropped into a flame. As the crushed glass melts, the surface tension molds it into a sphere which will then transform into an amorphous solid as it reaches the cooler region [31]. Figure 3 shows the fabricated microspheres and fiber under a microscope. A microsphere of diameter 70 μm, and fiber of diameter 83 μm were selected to perform the temperature calibrations described in the next section.

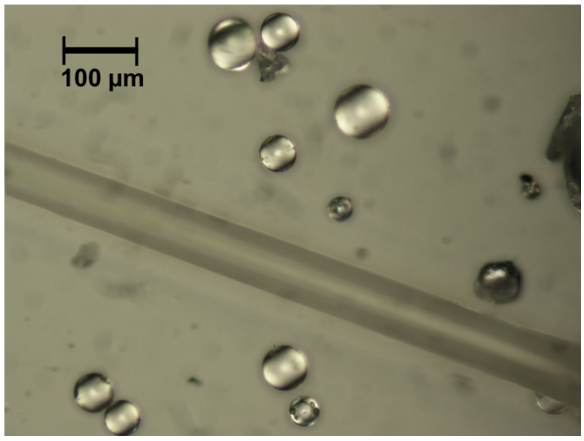

Figure 3. Optical image of the microspheres and optical fiber used in this work.

4.2 Experimental setup

4.2.1 WGM displacement calibration

The emission spectra of the samples were obtained using the experimental setup presented in Figure 4. A continuous 532 nm Nd: YAG laser (LS) was used in order to excite the sample and the emission spectrum was obtained from two different spectrographs, the SR-303i-B(SM1) coupled with a Newton 970EMCCD Camera and the SR-500i-B2(SM2) coupled with an Andor iDusInGaAs 1.7 μm. First, the laser beam passes through a short-pass filter (SP) singling out the 532 nm line and is diverted by a 45º mirror (M1) through a converging lens (L1) with f = 3 cm focusing on the pinhole (P) and dispersing towards another converging lens (L) with f = 15 cm. The resulting collimated beam is once again diverted by a 45º dichroic mirror (DM) towards a 20x

microscope objective (MO) which focalizes on the sample (S) placed on a three-dimensional translational stage. The emitted light from the sample travels towards a beam splitter that directs part of it to a long-pass filter and into a CCD camera (C) that shows a real-time image of the sample with the LED source illuminating the sample. This real-time image helps in positioning the sample to the focal point of the MO and also in estimating its size. The other part is directed back to the DM, passes through a long-pass filter eliminating possible second-harmonics of the excitation source and is focalized by a lens with f = 30 cm. The collimated emission beam is finally diverted by another 45º mirror (M2) towards the entrance slit of SM1 to obtain the emission spectrum of the sample in the visible region. The infrared spectrum is obtained by removing M2 in such a way that the collimated emission beam focalizes on the optical fiber connected to the entrance slit of SM2.

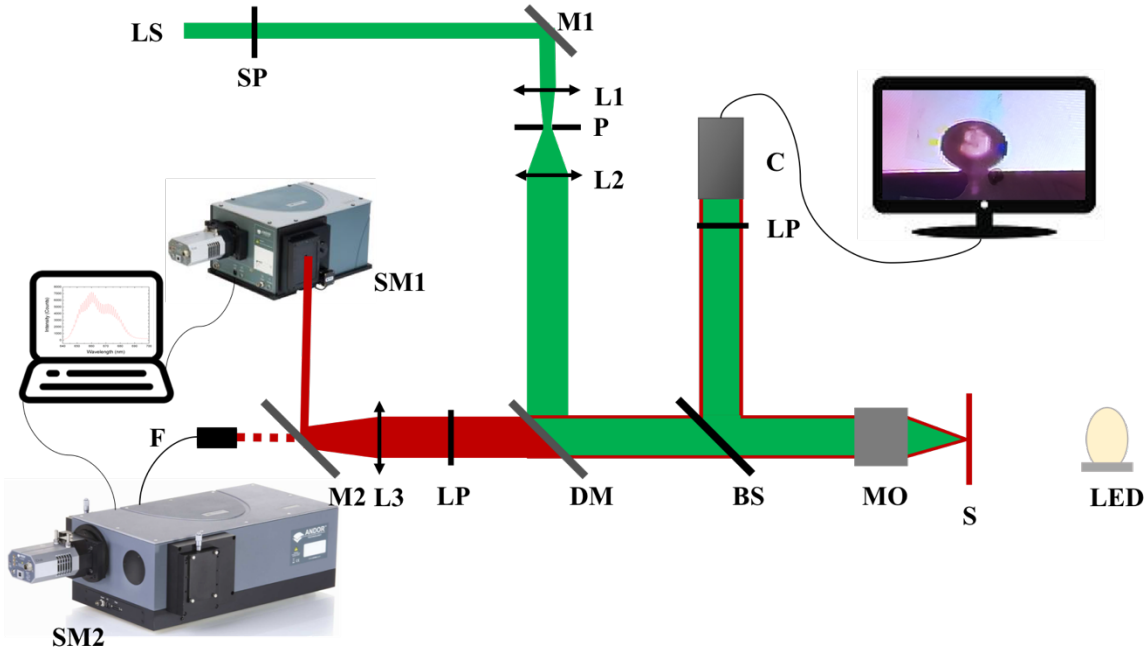

Figure 4. Confocal microluminiscence setup used to obtain the emission spectra of the excited samples.

As reported by L. L. Martín, the highest WGM resonance amplitudes were obtained by exciting at the center of the sample (microsphere or fiber) with the help of the translational stage and detecting at its borders by manipulating the inclination of M2 or the position of F [33].

Using this setup, two calibrations of the WGM resonant peak shifts were done. The first one involved heating the sample by increasing the power of the laser from 3 mW to 118 mW and obtaining the emission spectrum of the sample for every pump power. This allows an analysis of the relationship between the WGM shift and the pump power for different emission bands.

The second one involved heating the sample using a water bath heater with the excitation laser at low power. A thermocouple is placed near the sample indicating its temperature. The emission spectrum for each temperature from 294 K to 321 K were obtained permitting the temperature calibration of the WGM shifts. Due to the great complexity of the experimental setup, it was only done for one emission band of the microsphere sample. Furthermore, this calibration was not done for the fiber due to its low quality WGM peaks.

4.2.2 FIR temperature calibration

The temperature calibration of the bulk glass was done using the experimental setup shown in Figure 5. The bulk glass sample was placed in the middle of a tubular horizontal oven with a thermocouple located nearest to it as possible. Similar to the previous setup, a continuous 532 nm Nd:YAG laser (LS) was used to excite the sample by focalizing on it with the use of a converging lens (L1) with f = 20 cm. With another converging lens (L2) with f = 60 cm situated at the other end of the oven, the emitted light from the sample is focalized and then filtered by a long-pass filter into an optical fiber connected to a similar spectrograph as SM1 but coupled with a Newton 920 CCD Camera.

For the temperature calibration, the sample was heated from 297 K to 587 K and the corresponding emission spectra were recorded and analyzed.

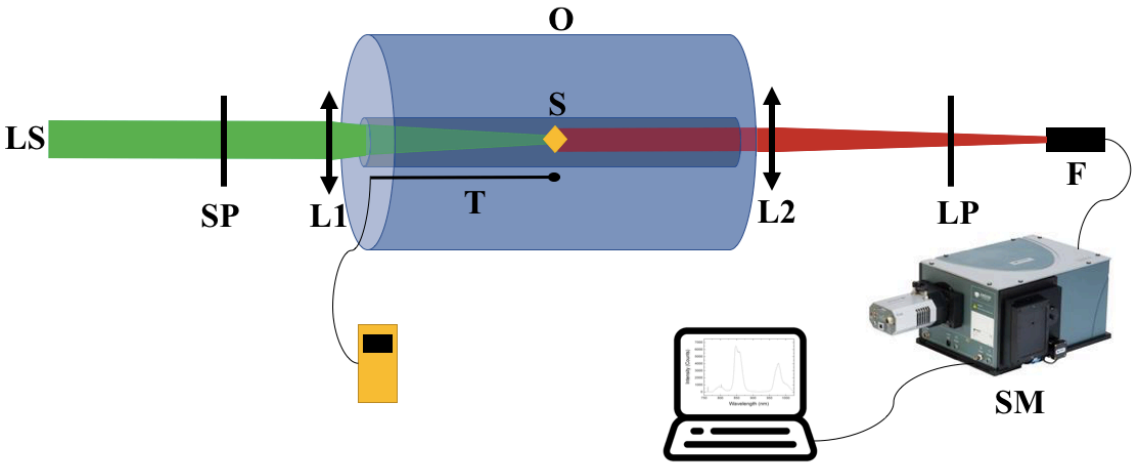

Figure 5. Experimental setup used for the FIR technique.

5. RESULTS AND DISCUSSION

En esta sección se presentarán y se analizarán los resultados obtenidos a partir de los procedimientos experimentales. Las bandas de emisión del vidrio de oxifluoruro dopado con Er^{3+} observadas se identificaron con las siguientes transiciones: 670 nm ($^4F_{9/2}\rightarrow{}^4I_{15/2}$), 800 nm ($^2H_{11/2}\rightarrow{}^4I_{13/2}$), 850 nm ($^4S_{3/2}\rightarrow{}^4I_{13/2}$), 975 nm ($^4I_{11/2}\rightarrow{}^4I_{15/2}$), and at 1550 nm ($^4I_{13/2}\rightarrow{}^4I_{15/2}$). Además, se compararon los espectros obtenidos de la microesfera, de la fibra óptica y del vidrio y se observaron resonancias de WGM para la microesfera y la fibra. A continuación, se obtuvieron los desplazamientos promedios de varios WGM producidos por la variación en la potencia del láser para cada banda de emisión de una microesfera de 70 µm y para una única banda de una fibra de 83 µm. Para la banda de 850 nm de la microesfera también se obtuvo el desplazamiento en función de la temperatura. Mediante la técnica FIR se determinó una separación de energía de 635 cm^{-1} entre los niveles térmicamente acoplados $^2H_{11/2}$ y $^4S_{3/2}$. Se encontró que la sensibilidad relativa del vidrio es dos órdenes de magnitud mayor que la de la microesfera, sin embargo, la incertidumbre en la temperatura resultó ser un orden de magnitud mayor. Esto implica que las medidas de temperatura que proporciona esta técnica son menos precisas que las medidas con el WGM.

The results obtained from the experimental procedures will be presented and analyzed in this section. The emission bands of the Er^{3+} doped oxyfluoride glass observed were identified with the corresponding transition as follows: 670 nm ($^4F_{9/2}\rightarrow{}^4I_{15/2}$), 800 nm ($^2H_{11/2}\rightarrow{}^4I_{13/2}$), 850 nm ($^4S_{3/2}\rightarrow{}^4I_{13/2}$), 975 nm ($^4I_{11/2}\rightarrow{}^4I_{15/2}$), and at 1550 nm ($^4I_{13/2}\rightarrow{}^4I_{15/2}$). Furthermore, the spectra from the microsphere, optical fiber, and bulk glass were compared and WGM resonances were observed for the microsphere and fiber. Afterwards, the WGM displacement rates due to the variation of the pump power for each emission band were obtained for a 70 µm microsphere and for one of the bands of an 83 µm fiber. From the 850 nm band of the microsphere, displacement rate as a function of temperature was also obtained. Through the FIR technique, an energy gap of 635 cm^{-1} was estimated between the thermally coupled levels $^2H_{11/2}$ and $^4S_{3/2}$. The relative sensitivity of the bulk glass was found out to be two orders of magnitude greater than that of the microsphere, while the temperature uncertainty obtained was an order of magnitude higher. This implies less precise measurements of temperature using the FIR technique compared with WGM analysis.

5.1 Emission spectrum of Erbium

The emission spectra of an Er^{3+} doped oxyfluoride glass in the form of a microsphere, optical fiber, and bulk material are shown in Figure 6. These spectra were obtained under the excitation of the samples with a continuous 532 nm laser. The characteristic emission bands of Er^{3+} are observed at 670 nm ($^4F_{9/2}\rightarrow{}^4I_{15/2}$), 800 nm

($^2H_{11/2}\rightarrow{}^4I_{13/2}$), 850 nm ($^4S_{3/2}\rightarrow{}^4I_{13/2}$), 975 nm ($^4I_{11/2}\rightarrow{}^4I_{15/2}$), and at 1550 nm ($^4I_{13/2}\rightarrow{}^4I_{15/2}$). A schematic energy level diagram of Er^{3+} showing the aforementioned transitions is presented in Figure 7. The 800 nm and 850 nm emission bands lie within the first biological window (650 nm – 1000 nm), thus the thermal calibration of these bands can have various biomedical applications [34].

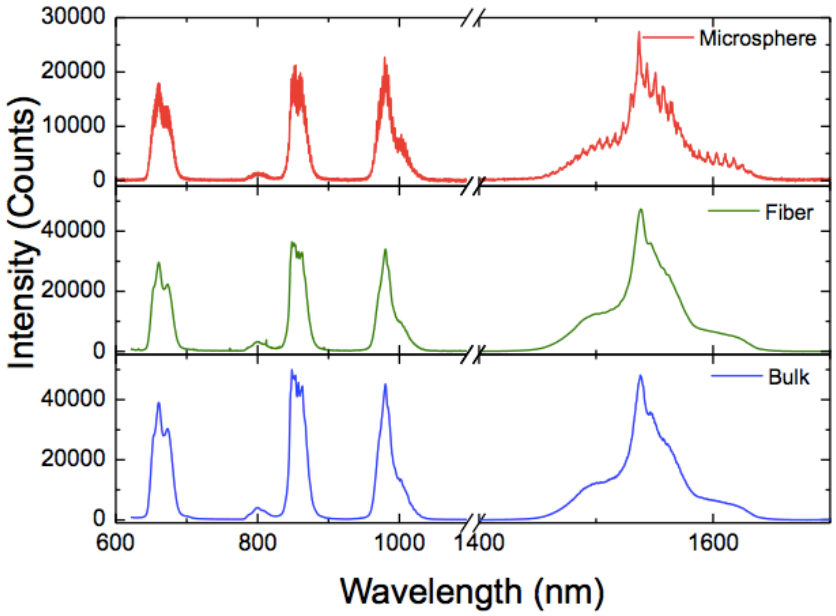

Figure 6. Emission spectra of Er^{3+} doped oxyfluoride glass in the form of microsphere, optical fiber, and bulk material, under the excitation at 532 nm. The spectra from 600 nm to 1100 nm are amplified by a factor 25.

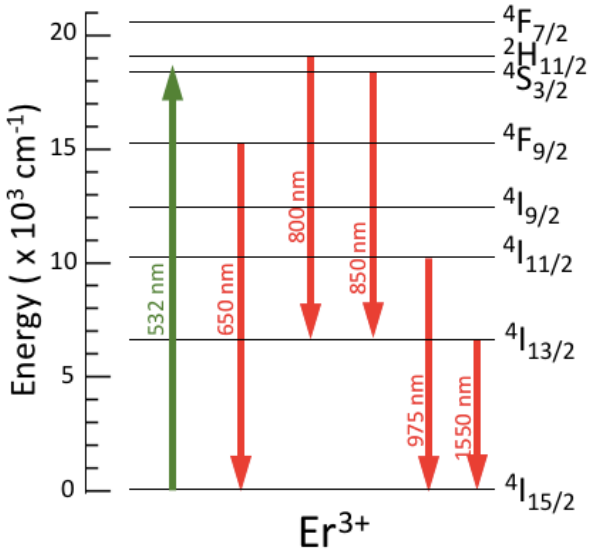

Figure 7. Partial energy level diagram of Er^{3+}indicating the transitions observed under the 532 nm excitation [30,35].

For the microsphere and optical fiber, the laser was directed at the center of the samples and the spectrum detection zone was placed at their borders, and the WGM

resonances superimposed on the Er^{3+} spectra were observed. The 670 nm band was selected from Figure 6 and normalized in Figure 8 in order to compare the WGM resonances from each sample. As expected, the bulk material does not present WGM due to its lack of a closed concave surface. On the other hand, the spherical and cylindrical shape of the microsphere and optical fiber respectively, contributes to the manifestation of WGM. The microsphere and fiber WGM peaks both have a full width at half maximum (FWHM) about 0.5 nm. However, it can be observed that the WGM resonances in the microsphere are much more prominent than those of the optical fiber since it has more concave surfaces, thus trapping the light longer in its interior producing higher amplitude of the resonances. Given that a higher signal implies a better signal-to-noise ratio, this suggests that the microsphere is more suitable to be used as a temperature sensor than the fiber.

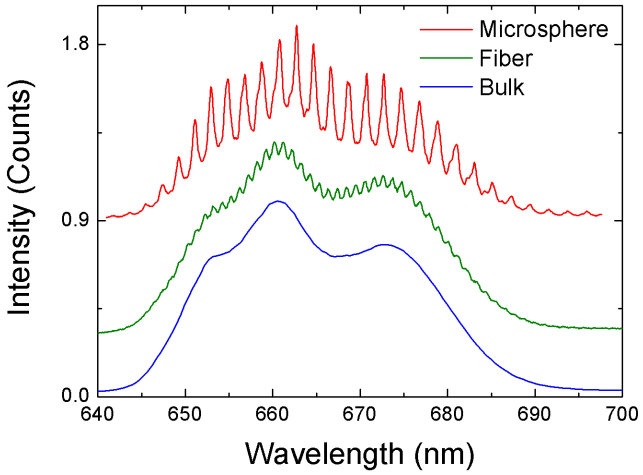

Figure 8. The emission band at 670 nm showing the resonances associated to the WGM. The intensity bands were normalized and displaced vertically for comparison purposes.

Moreover, the WGM peaks can be observed in all the emission bands of the microsphere and fiber. Therefore, the bands with higher intensity such as 670 nm, 850 nm, 975 nm, and 1550 nm were used for the study of WGM displacement as a function of pump power and the corresponding temperature calibration of the shifts for the microsphere. For the fiber, only the 975 nm band was studied for the pump power calibration.

5.2 Analysis of the WGM Displacement

5.2.1 WGM displacement as a function of laser pump power

In order to study the displacement of the WGM resonance peaks as a function of the laser pump power, a 70 µm diameter microsphere and an 83 µm diameter optical fiber were subjected to different pump powers from 3 mW to 118 mW and various spectra were recorded. For the microsphere, five peaks from each of the emission bands of 670 nm, 850 nm, 975 nm, and 1550 nm were selected and their positions in each spectrum were monitored. However, due to the weak WGM resonances of the optical fiber, only

the 975 nm emission band was considered through the same method. Figure 9 is obtained by averaging the shift of five peaks for each band and spectrum.

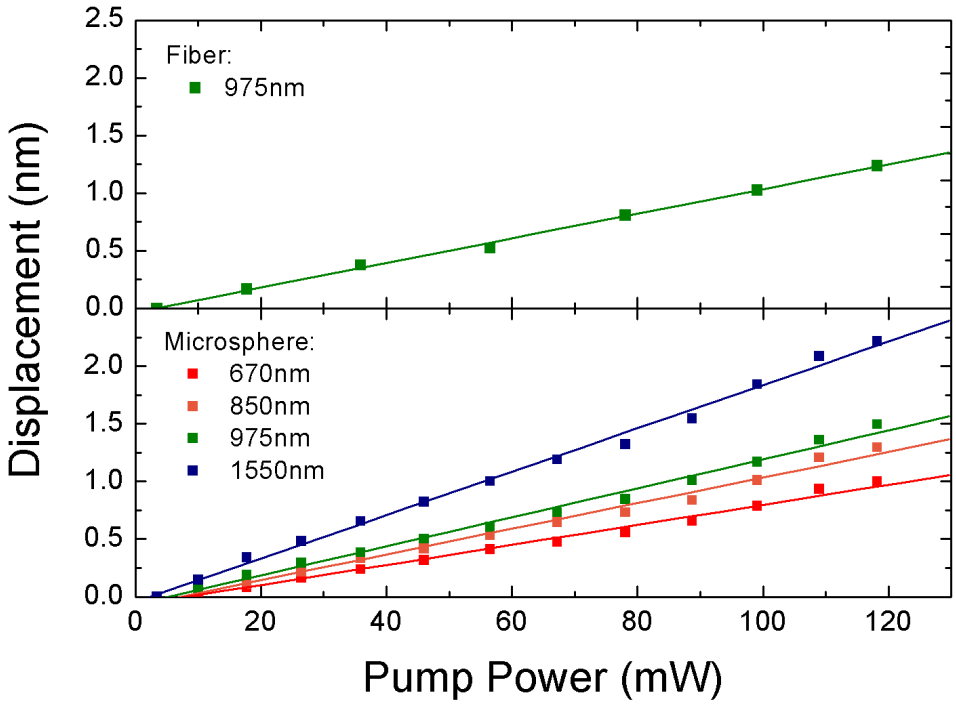

Figure 9. Displacement of the WGM peaks of the optical fiber and microsphere as a function of the laser pump power.

From Figure 9, a general shift to the higher wavelength region of the spectra is observed as the pump power increases. The experimental values show a linear tendency for each calibration suggesting that the displacement rate is independent of the pump power. A linear fitting for each emission band was done in order to calculate the average displacement rates and the fitted parameters are presented in Table 1. In the case of the 975 nm emission band of the fiber, displacement rate of 11 pm/mW was recorded while for the microsphere, displacement rates of 9 pm/mW, 11 pm/mW, 13 pm/mW, and 19 pm/mW were obtained for the 670 nm, 850 nm, 975 nm, and 1550 nm emission band respectively. The difference between the displacement rate of the fiber and microsphere for the same 975 nm emission band is attributed to the difference in the heating process of the laser pump power of each sample in the experimental setup and not because of their thermal properties.

	Fiber	**Microsphere**			
$\Delta\lambda = A * P + B$	975 nm	670 nm	850 nm	975 nm	1550 nm
A (nm/mW)	0.011	0.009	0.011	0.013	0.019
B (nm)	-0.031	-0.071	-0.078	-0.065	-0.044

Table 1. Linear fit parameters of WGM displacements as a function of pump power

It can also be inferred from the graph that for all the emission bands, the shift does not start immediately, not until a certain pump power is applied. This shows that the heating process is not relevant a determined pump power is reached.

The displacement rates for each emission band of the microsphere are represented in Figure 10. This suggests that there is a linear and direct relationship between the displacement rate of the WGM peaks and the wavelength. Therefore, a bigger shift is to be expected for longer wavelengths.

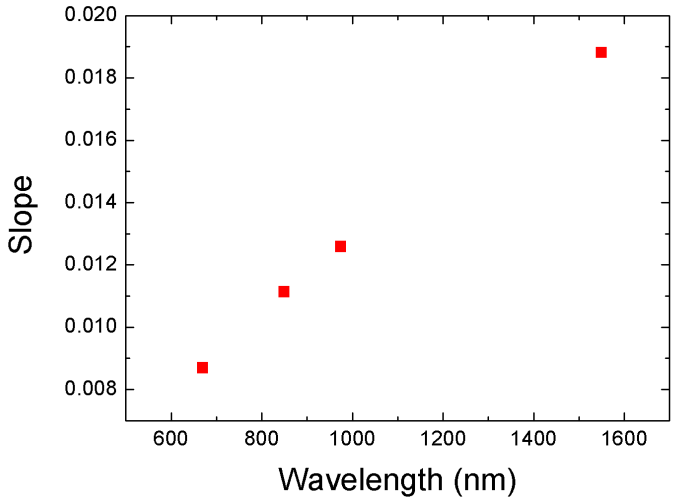

Figure 10. Displacement rates of the WGM peaks of the microsphere due to the change in laser pump power for each emission band of Er^{3+}

5.2.2 WGM displacement as a function of temperature

In order to calibrate the temperature, a 70 µm diameter microsphere was heated from 294 K to 321 K using a water bath heater and the successive spectra were obtained. A data analysis similar to the procedure used in the previous section was done for the 850 nm emission band of the microsphere to obtain the variation in the WGM peak position with temperature as shown in Figure 11. By linear fitting, an average displacement rate of 84 pm/K is obtained. This value is greater than the 11 pm/K observed for a silica microsphere in literature [12]. By using this calibration, and knowing that the total shift of the 850 nm band (see Figure 9) is 1.3 nm, the temperature corresponding to the 118 mW pump power is estimated to be 310 K.

Taking into account that the α and β in Equation (4) do not depend on the wavelength, these values can be estimated from the calibration shown in Figure 11 and then used to calculate the displacement rates for the other bands of the microsphere. Displacement rates of 66 pm/K, 96 pm/K, and 153 pm/K were obtained for the 670 nm, 975 nm, and 1550 nm band respectively.

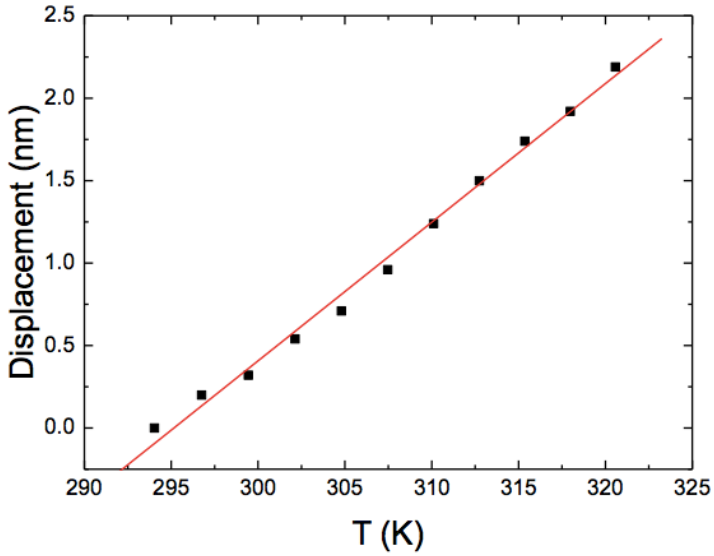

Figure 11. Displacement of WGM peaks of the 850 nm band of the microsphere as a function of temperature. The solid line corresponds to the fit $\Delta\lambda(nm) = 0.084\,T - 25$.

5.2.3 Contribution of thermal expansion and refraction index change to the WGM displacement

As stated in Chapter 3, the shift of the WGM resonances with temperature is the result of two phenomenon: the change in the dimensions of the sample represented by α, and the change in the refraction index of the material represented by β. In this subsection, the contributions of each effect to the observed WGM displacement will be analyzed.

The thermal expansion coefficient of the oxyfluoride glass is unknown. Instead, the α for an oxyfluoride glass with similar composition obtained by Krishnaiah [36] will be used for this analysis. This similar glass has a composition (in mol%): 30 SiO_2, 15 Al_2O_3, 27 CdF_2, 22 PbF_2, 4 YF_3, and 2 YbF_3 with $\alpha = 11.3 \times 10^{-6}\ K^{-1}$. The contribution of the thermal expansion to the WGM displacement for the 850 nm band obtained in Figure 11 was calculated by introducing this value in Equation (4) and represented in Figure 12. Comparing this contribution with the total observed WGM shift, it can be concluded that the WGM displacements occur primarily not because of the thermal expansion but because of the change in the refraction index. Using the fitted parameters of the experimental data and the slope of the α contribution, the β for this glass is estimated to be $\beta = 8.14 \times 10^{-5}\ K^{-1}$.

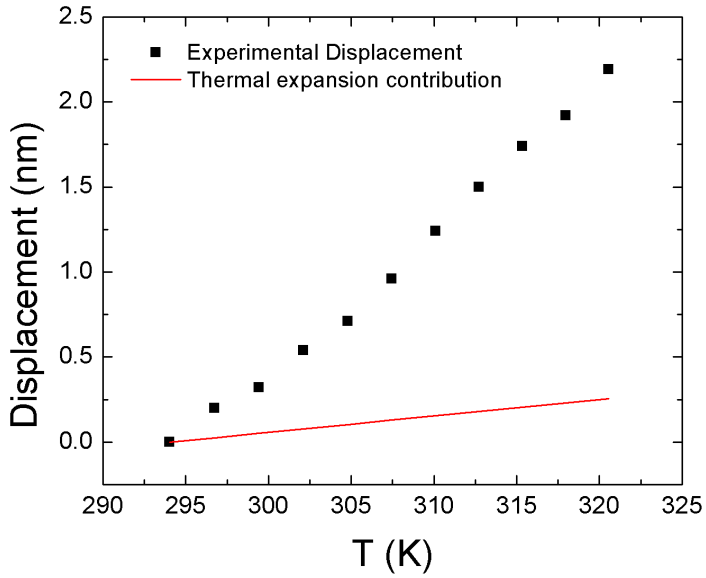

Figure 12. Thermal expansion contribution to the WGM displacements compared to the experimental results

5.3 Fluorescence Intensity Ratio (FIR)

The FIR technique was used to calibrate the behavior with temperature of an Er^{3+} doped oxyfluoride bulk glass. For this, the bulk material was heated from 297 K to 587 K and the successive emission spectra were obtained. Due to the proximity of the $^2H_{11/2}$ and $^4S_{3/2}$ energy levels, a thermal population redistribution occurs. Thus, this method consists of analyzing the ratio of the areas of the associated emission bands, 800 nm and 850 nm, as a function of the temperature of the sample. Figure 13 shows the experimental values obtained for the ratio at certain temperatures. It can be observed that as the temperature rises, the area of the 800 nm band also increases with respect to that of the 850 nm band. This verifies what was initially commented on Chapter 3. As the temperature increases, the vibration of the phonons in the host material increases and they interact with the erbium ions in order to promote the ones from the $^4S_{3/2}$ level to the $^2H_{11/2}$ level, thus, increasing the 800 nm band intensity with respect to the 850 nm band. The experimental values are then fitted to Boltzmann distribution (see Equation (5)) and an energy gap of 635 cm^{-1} is obtained.

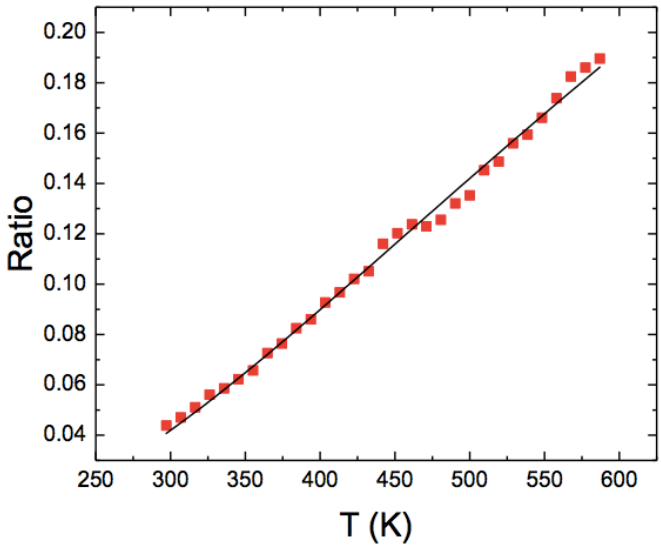

Figure 13. Ratio of the thermally coupled emission bands of Er^{3+} as a function of the bulk sample temperature. Parameters of the fit to Equation (5) are ΔE = 635 cm^{-1} and B = 0.88.

5.4 Sensor performance of the microsphere, fiber, and bulk glass

To compare the performance of the microsphere, fiber and bulk glass as temperature sensors, two parameters will be estimated: relative sensor sensitivity and temperature uncertainty.

5.4.1 Relative sensor sensitivity

Relative sensor sensitivity, defined by Equation (6), has been particularized to the WGM and FIR techniques leading to Equations (7) and (8).

The variation of the WGM wavelength with temperature was represented by Figure 11, being the slope of the linear fit the term $(\alpha + \beta)\lambda$. This slope allows the estimation of the relative sensitivity, which for the 850 nm band of the microsphere has a value of 9.9 x 10^{-5} K^{-1}. As α and β do not depend on the wavelength, according to Equation (7), the relative sensitivity is also independent of the wavelength, thus, the same relative sensitivity will be obtained for the rest of emission bands. Moreover, as α and β are also independent of the morphology of the material, the fiber has the same relative sensitivity as the microsphere. For comparison, a relative sensitivity of 5.3 x 10^{-6} K^{-1} was observed for a silica fiber as reported in Ref [37].

The relative sensitivity S_{FIR} of the bulk glass using the FIR technique is calculated using the fitted parameters of Figure 13 through Equation (8) and is represented in Figure 14. The maximum sensitivity was obtained for the lowest temperature with a value of S_{FIRmax} = 1.0 x 10^{-2} K^{-1}. This is similar to the sensitivity measured in an Er^{3+}/Yb^{3+} doped

$LaGdO_3$ glass as reported in Ref [19]. It can be seen that the bulk glass has a significantly higher value of sensitivity than the microresonators.

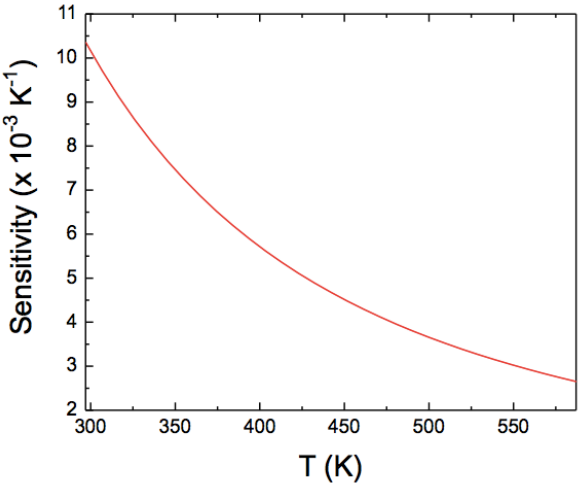

Figure 14. Relative sensitivity S_{FIR} of the bulk glass

5.4.2 Temperature uncertainty

Temperature uncertainties for the WGM and FIR techniques were experimentally estimated by measuring 100 spectra under the same experimental conditions. In the case of WGM technique, the position of a WGM peak was estimated for each of the 100 spectra (both for the microsphere and the fiber) by calculating the centroid of one WGM peak. The variance of the centroid was calculated and the distribution of the centroid positions for the microsphere was represented in Figure 15. The peak position uncertainty $\delta\lambda$ was taken as the standard deviation and is 0.007 nm for the microsphere and 0.025nm for the fiber. The uncertainty in the WGM position of the microsphere is about 1% of the FWHM of the peak as reported by F. Vollmer [38]. However, the uncertainty for the fiber is larger than predicted by F. Vollmer due to the low quality of the peaks. The temperatures corresponding to the WGM peak position of the microsphere and fiber were estimated from the calibration for each of the 100 measurements and the resulting temperature distribution is represented in Figure 15. The temperature uncertainty was estimated as the standard deviation of the temperature distribution having a value of 0.11 K for the microsphere and 0.37 K for the fiber, both corresponding to the 670 nm band.

In the FIR technique, the distribution of intensity ratios of the 100 measured spectra was obtained and represented in Figure 15, as well as the temperature distribution inferred from the calibration curve. The uncertainty in the ratio of intensities δR is 7.7 x 10^{-4} and the temperature uncertainty is 1.8 K.

As can be seen from Figure 15, the distribution of temperature is significantly wider for the FIR method.

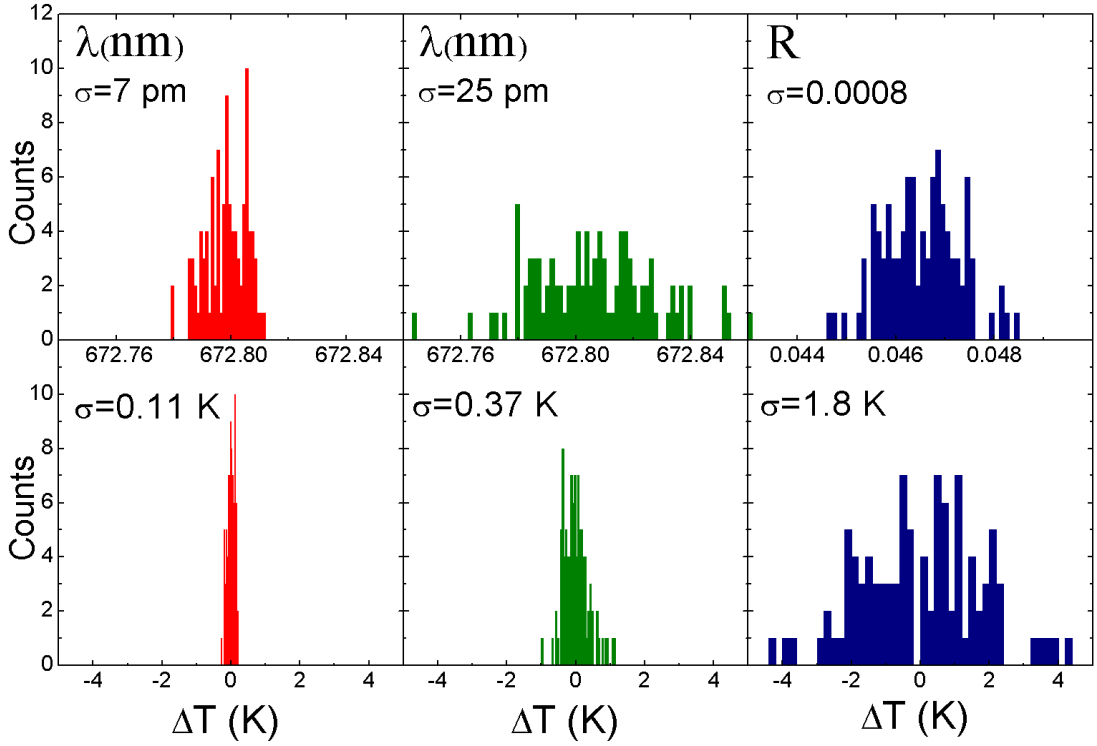

Figure 15. Distribution of the measured parameters (i.e. wavelength, ratio) for microsphere (red), fiber (green) and bulk glass (blue), the corresponding temperature distribution obtained from the WGM displacement analysis and FIR technique for the three samples.

Temperature uncertainties for the rest of emission bands of the microsphere and fiber were estimated from the value obtained for the 670 nm band, using Equation (9). It has been taken into account that $\delta\lambda$ is characteristic of the experimental setup, thus, independent of the wavelength. The temperature uncertainties obtained for the 850 nm, 975 nm, 1550 nm band are 0.09 K, 0.08 K, and 0.05 K respectively for the microsphere, and 0.29 K, 0.25 K, and 0.16 K respectively for the fiber.

Sensor Parameter	Microsphere	Optical Fiber	Bulk Glass
Relative sensitivity (K^{-1})	9.9×10^{-5}	9.9×10^{-5}	1.0×10^{-2}
Temperature uncertainty (K)	**670 nm:** 0.11 **850 nm:** 0.09 **975 nm:** 0.08 **1550 nm**: 0.05	**670 nm:** 0.37 **850 nm:** 0.29 **975 nm:** 0.25 **1550 nm**: 0.16	1.8

Table 2. Sensor parameters of the three morphologies of Er^{3+} doped oxyfluoride glass

The sensor parameters obtained for the three forms of Er^{3+} doped oxyfluoride glass are summarized in Table 2. A similar temperature uncertainty for WGM (δT = 0.1 K) and FIR (δT = 1 K) were obtained in the literature [14] for a Nd^{3+} doped barium titano silicate microsphere and bulk glass. It can be observed that the relative sensitivity of the WGM based sensors (i.e. microsphere and fiber) are two orders of magnitude lower than

that of the FIR based sensor (i.e. bulk glass). On the other hand, the temperature uncertainty from the WGM analysis of microsphere and fiber is an order of magnitude lower than that obtained by the FIR method. This implies that among the two sensing methods employed, sensing through WGM displacement analysis provides more precise temperature measurements. For the two morphologies considered, being the microsphere the best choice due to its lower temperature uncertainty.

6. CONCLUSIONS

A través de este trabajo, se ha llegado a la conclusión de que la detección de temperatura a través del análisis de los desplazamientos de los WGM de un microresonador proporciona medidas de temperatura más precisas que la técnica FIR del vidrio con una forma genérica. Además, entre una microesfera y una fibra, se encontró que esta primera proporciona medidas de temperatura con mayor precisión. Por otro lado, la técnica FIR ofrece una mayor sensibilidad relativa que la de los sensores basados en WGM. Este trabajo ha abierto una variedad de nuevas ideas y problemas que pueden ser explorados en estudios futuros.

Through this work, it has been concluded that temperature sensing through the WGM displacement analysis provides more precise temperature measurements in comparison with the FIR technique of the bulk glass. Moreover, among the microresonators studied, the microsphere proved to be better than the fiber in terms of temperature uncertainty. On the other hand, the FIR technique offers higher relative sensitivity than those of the WGM based sensors. This work has opened a variety of new ideas and problems that can be explored in future studies.

Three samples of different morphologies (i.e. microsphere, fiber, and bulk glass) were fabricated from the same precursor glass of Er^{3+} doped oxyfluoride glass and studied in order to determine their thermal sensing capabilities. The emission bands centered in 670 nm, 800 nm, 850 nm, 975 nm, and 1550 nm obtained when the samples are excited with a 532 nm laser were identified as the following transitions of the Er^{3+} ions: $^4F_{9/2}\rightarrow{}^4I_{15/2}$, $^2H_{11/2}\rightarrow{}^4I_{13/2}$, $^4S_{3/2}\rightarrow{}^4I_{13/2}$, $^4I_{11/2}\rightarrow{}^4I_{15/2}$, and $^4I_{13/2}\rightarrow{}^4I_{15/2}$ respectively.

WGM peaks were observed for the microsphere and fiber using a confocal microluminiscence setup by exciting the sample at the center and placing the detection zone at the border. The WGM peaks of the microsphere have much higher amplitudes than that of the fiber, thus, a higer signal-to-noise ratio is to be expected for the microsphere. As an effect of a temperature change either by heating with the laser or with a water bath, the WGM peaks were observed to shift towards the red region of the spectra. Thus, the study of the thermal sensing capability of the microsphere and fiber were executed using the WGM displacement principle.

A calibration of the WGM displacement as a function of the pump power was done and displacement rates of 9 pm/mW, 11 pm/mW, 13 pm/mW, and 19 pm/mW were obtained for the 670 nm, 850 nm, 975 nm, and 1550 nm emission bands of the microsphere respectively and 11 pm/mW for the 975 nm band of the fiber. A similar calibration of the displacements as a function of temperature was performed for the 850 nm band of the microsphere and a displacement rate of 84 pm/K was observed. The displacement rates for the 670 nm, 975 nm, and 1550 nm emission bands were inferred

pseudo-experimentally and the following values were obtained: 66 pm/K, 96 pm/K, and 153 pm/K. It can be concluded that the displacement rate increases with the wavelength as predicted by Equation (3). Furthermore, from the estimation of the thermal expansion and thermo-optic contributions, it was determined that the major factor influencing the WGM displacements is the change in the refraction index of the material with temperature.

The thermalization effect in the $^{2}H_{11/2}$ and $^{4}S_{3/2}$ energy levels of Er^{3+} was studied through the FIR technique. The ratio of the integrated areas of the 800 nm and 850 nm bands as a function of temperature were fitted to the Boltzmann distribution and an energy gap of 635 cm^{-1} was obtained.

In order to compare the sensor performance of the three samples, the relative sensitivities and temperature uncertainties were determined. A relative sensitivity of 9.9 x 10^{-5} K^{-1} was obtained for the microsphere and for the fiber while the bulk glass presented a relative sensitivity two orders of magnitude higher, 1.0 x 10^{-2} K^{-1}. The temperature uncertainties of the microsphere, fiber and bulk glass were estimated experimentally. The temperature uncertainties of the microsphere and fiber are an order of magnitude lower than that of the bulk glass, with the microsphere having the lowest value of the temperature uncertainty.

In conclusion, it can be said that WGM displacement analysis of the microsphere provides temperature measurements with higher precision than the WGM displacement analysis of the fiber and FIR method.

The calibration of the other emission bands of the microsphere with temperature will be considered as future work. The temperature calibration of the WGM displacements of the fiber will need a more stable and low noise experimental setup due to the lower value of the signal-to-noise ratio.

Furthermore, a similar temperature calibration for a microsphere glued at the end of a transparent fiber can be performed. In this case, the microsphere will be excited through the fiber and its response detected through the same fiber.

On the other hand, the fact that the 800 nm and 850 nm emission bands of Er^{3+} lie in the first biological window, opens another topic for future studies. Since it has been determined that temperature sensing using microsphere provides higher precision measurements, it would be interesting to do a similar temperature calibration for the 850 nm band but exciting the sample in the infrared region. Moreover, the penetration depth in the human tissue of these emission bands can also be studied using phantom tissues.

7. BIBLIOGRAPHY

1. A. Rostami, H. Ahmadi, H. Heidarzadeh, and A. Taghipour, "Microsphere and Fiber Optics based Optical Sensors," Opt. Sensors - New Dev. Pract. Appl. (2014).
2. V. K. Rai, "Temperature sensors and optical sensors," Appl. Phys. B Lasers Opt. **88**(2), 297–303 (2007).
3. N. M. Hanumegowda, I. M. White, and X. Fan, "Aqueous mercuric ion detection with microsphere optical ring resonator sensors," Sensors Actuators, B Chem. **120**(1), 207–212 (2006).
4. S. A. Wade, "Temperature Measurement Using Rare Earth Doped Fibre Fluorescence," (1999).
5. M. Bass and W. Koechner, *Solid-State Lasers : A Graduate Text* (2002).
6. S. Tanabe, "Optical transitions of rare earth ions for amplifiers: How the local structure works in glass," J. Non. Cryst. Solids **259**(1–3), 1–9 (1999).
7. S. Tanabe, S. Yoshii, K. Hirao, and N. Soga, "Upconversion properties, multiphonon relaxation, and local environment of rare-earth ions in fluorophosphate glasses," Phys. Rev. B **45**(9), 4620–4625 (1992).
8. S. Tanabe, H. Hayashi, T. Hanada, and N. Onodera, "Fluorescence properties of Er3+ ions in glass ceramics containing LaF3 nanocrystals," Opt. Mater. (Amst). **19**(3), 343–349 (2002).
9. L. Feng, J. Wang, Q. Tang, L. Liang, H. Liang, and Q. Su, "Optical properties of Ho3+-doped novel oxyfluoride glasses," J. Lumin. **124**(2), 187–194 (2007).
10. A. Jain and K. E. Goodson, "Thermal microdevices for biological and biomedical applications," J. Therm. Biol. **36**(4), 209–218 (2011).
11. G. Guan, S. Arnold, and M. V. Otugen, "Temperature measurements using a microoptical sensor based on whispering gallery modes," AIAA J. **44**(10), (2006).
12. Q. Ma, T. Rossmann, and Z. Guo, "Whispering-gallery mode silica microsensors for cryogenic to room temperature measurement," Meas. Sci. Technol. **21**(2), (2010).
13. C. H. Dong, L. He, Y. F. Xiao, V. R. Gaddam, S. K. Ozdemir, Z. F. Han, G. C. Guo, and L. Yang, "Fabrication of high- Q polydimethylsiloxane optical microspheres for thermal sensing," Appl. Phys. Lett. **94**(23), (2009).
14. L. L. Martín, C. Pérez-Rodríguez, P. Haro-González, and I. R. Martín, "Whispering gallery modes in a glass microsphere as a function of temperature," Opt. Express **19**(25), 25792 (2011).
15. Q. Ma, T. Rossmann, and Z. Guo, "Temperature sensitivity of silica micro-resonators," J. Phys. D. Appl. Phys. **41**(24), (2008).
16. C. Pérez-Rodríguez, L. L. Martín, S. F. León-Luis, I. R. Martín, K. K. Kumar, and C. K. Jayasankar, "Relevance of radiative transfer processes on Nd3+ doped phosphate glasses for temperature sensing by means of the fluorescence intensity ratio technique," Sensors Actuators, B Chem. **195**, 324–331 (2014).
17. W. Xu, H. Zhao, Y. Li, L. Zheng, Z. Zhang, and W. Cao, "Optical temperature sensing through the upconversion luminescence from Ho3+/Yb3+ codoped

CaWO4," Sensors Actuators, B Chem. **188**, 1096–1100 (2013).
18. V. K. Rai and C. B. de Araujo, "Fluorescence intensity ratio technique for Sm3+ doped calibo glass," Spectrochim. Acta - Part A Mol. Biomol. Spectrosc. **69**(2), 509–512 (2008).
19. A. Siaï, P. Haro-González, K. Horchani Naifer, and M. Férid, "Optical temperature sensing of Er3+/Yb3+doped LaGdO3based on fluorescence intensity ratio and lifetime thermometry," Opt. Mater. (Amst). **76**, 34–41 (2018).
20. H. Berthou and C. K. Jörgensen, "Optical-fiber temperature sensor based on upconversion-excited fluorescence," Opt. Lett. **15**(19), 1100 (1990).
21. T. Ioppolo and M. V. Ötügen, "Pressure tuning of whispering gallery mode resonators," J. Opt. Soc. Am. B **24**(10), 2721 (2007).
22. L. Labrador-Páez, K. Soler-Carracedo, M. Hernández-Rodríguez, I. R. Martín, T. Carmon, and L. L. Martin, "Liquid whispering-gallery-mode resonator as a humidity sensor," Opt. Express **25**(2), 1165 (2017).
23. G. C. Righini, Y. Dumeige, P. Féron, M. Ferrari, G. N. Conti, D. Ristic, and S. Soria, "Whispering Gallery Mode microresonators: Fundamentals and applications," Riv. del Nuovo Cim. **34**(7), 435–488 (2011).
24. F. Foreman, Matthew R., Swaim, Jon D., Vollmer, "Whispering gallery mode sensors," Adv. Opt. Photonics **7**(2), 168–240 (2015).
25. G. Ghosh, "Model for the Thermooptical Coefficients of Some Standard Optical-Glasses," J. Non. Cryst. Solids **189**(1–2), 191–196 (1995).
26. D. S. Sanditov and B. S. Sydykov, "Modulus of elasticity and thermal expansion coefficient of glassy solids," Phys. Solid State **56**(5), 1006–1008 (2014).
27. S. F. Collins, G. W. Baxter, S. A. Wade, T. Sun, K. T. V. Grattan, Z. Y. Zhang, and A. W. Palmer, "Comparison of fluorescence-based temperature sensor schemes: Theoretical analysis and experimental validation," J. Appl. Phys. **84**(9), 4649–4654 (1998).
28. S. A. Wade, S. F. Collins, and G. W. Baxter, "Fluorescence intensity ratio technique for optical fiber point temperature sensing," J. Appl. Phys. **94**(8), 4743–4756 (2003).
29. C. D. S. Brites, A. Millán, and L. D. Carlos, "Lanthanides in Luminescent Thermometry," in *Handbook on the Physics and Chemistry of Rare Earths* (2016), **49**, pp. 339–427.
30. J. Mendez-Ramos, V. Lavin, I. R. Martin, U. R. Rodriguez-Mendoza, J. A. Gonzalez-Almeida, V. D. Rodriguez, A. D. Lozano-Gorrin, and P. Nunez, "Optical properties of Er 3+ ions in transparent glass ceramics," J. Alloys Compd. **323–324**, 753–758 (2001).
31. G. R. Elliott, D. W. Hewak, G. S. Murugan, and J. S. Wilkinson, "Chalcogenide glass microspheres; their production, characterization and potential," Opt. Express **15**(26), 17542–17553 (2007).
32. V. Lefèvre-Seguin, "Whispering-gallery mode lasers with doped silica microspheres," Opt. Mater. (Amst). **11**(2–3), 153–165 (1999).
33. L. L. Martín, P. Haro-González, I. R. Martín, D. Navarro-Urrios, D. Alonso, C. Pérez-Rodríguez, D. Jaque, and N. E. Capuj, "Whispering-gallery modes in glass

microspheres: optimization of pumping in a modified confocal microscope," Opt. Lett. **36**(5), 615 (2011).

34. H. Suo, F. Hu, X. Zhao, Z. Zhang, T. Li, C. Duan, M. Yin, and C. Guo, "All-in-one thermometer-heater up-converting platform YF_3:Yb^{3+},Tm^{3+} operating in the first biological window," J. Mater. Chem. C **5**(6), 1501–1507 (2017).
35. L. Radžiūtė, D. Kato, G. Gaigalas, P. Jönsson, P. Rynkun, V. Jonauskas, and S. Kučas, "Energy level structure of the ground configuration in the Er 3+ free ion," Phys. Scr. **90**(5), 054001 (2015).
36. K. V. Krishnaiah, E. S. De Lima Filho, Y. Ledemi, G. Nemova, Y. Messaddeq, and R. Kashyap, "Development of ytterbium-doped oxyfluoride glasses for laser cooling applications," Sci. Rep. **6**(January), 1–12 (2016).
37. E. Rivera-Pérez, I. L. Villegas, A. Díez, M. V. Andres, J. L. Cruz, and A. Rodríguez-Cobos, "Measurement of pump-induced temperature increase in doped fibers using whispering-gallery modes," IEEE Photonics Technol. Lett. **25**(24), 2498–2500 (2013).
38. F. Vollmer and S. Arnold, "Whispering-gallery-mode biosensing: Label-free detection down to single molecules," Nat. Methods **5**(7), 591–596 (2008).